Comparison of photoacoustic spectroscopy and cavity ring down spectroscopy for ambient methane monitoring at Hohenpeißenberg

Max Müller[1, 2], Stefan Weigl[1], Jennifer Müller-Williams[3], Matthias Lindauer[3], Thomas Rück[1], Simon Jobst[1, 2], Rudolf Bierl[1], and Frank-Michael Matysik[2]

[1]Sensorik-ApplikationsZentrum, University of Applied Sciences Regensburg, 93053 Regensburg, Germany
[2]Institute of Analytical Chemistry, Chemo- and Biosensors, University Regensburg, 93053 Regensburg, Germany
[3]Meteorological Observatory Hohenpeißenberg, Deutscher Wetterdienst, 82383 Hohenpeißenberg, Germany

Correspondence: Max Müller (max.mueller@oth-regensburg.de)

Abstract. With an atmospheric concentration of approximately 2000 parts per billion (ppbV, 10^{-9}) methane (CH_4) is the second most abundant greenhouse gas (GHG) in the atmosphere after carbon dioxide (CO_2). The task of long-term and spatially resolved GHG monitoring to verify whether climate policy actions are effective, is becoming more crucial as climate change progresses. In this paper we report the CH_4 concentration readings of our photoacoustic (PA) sensor over a five day period at Hohenpeißenberg, Germany. As a reference device a calibrated cavity ringdown spectrometer Picarro G2301 from the meteorological observatory of the German Weather Service (DWD) was employed. Trace gas measurements with photoacoustic instruments promise to provide low detection limits at comparably low costs. However, PA devices are often susceptible to cross-sensitivities related to fluctuating environmental conditions, e.g. ambient humidity. The obtained results show that for PA sensor systems non-radiative relaxation effects induced by varying humidity are a non-negligible factor. Applying algorithm compensation techniques, which are capable of calculating the influence of non-radiative relaxational effects on the photoacoustic signal, increase the accuracy of the photoacoustic sensor significantly. With an average relative deviation of 1.11 % from the G2301, the photoacoustic sensor shows good agreement with the reference instrument.

1 Introduction

In the European network Integrated Carbon Observation System (ICOS) 16 different nations united to measure greenhouse gas (GHG) concentrations continuously in the atmosphere and in a standardized way. In order to ensure data comparability of the 46 atmosphere monitoring stations the required accuracy of the devices were defined in the ICOS program. For CH_4 this was specified to be less than ± 2 ppbV, emphasising the high standards set internationally for reliable atmospheric GHG monitoring (ICOS RI, 2020). For this purpose a state-of-the-art cavity ringdown spectrometer G2301 (Picarro, Inc.,USA) was selected by the ICOS program for both CH_4 and CO_2 quantification, which provides a 3σ precision for CH_4 less than 1.5 ppbV and less than 210 ppbV for CO_2 at an averaging time of 5 seconds. For leakage detection of gas pipelines, or identification of various methane sources, measurement instruments with slightly lower precision may also be appropriate. In 2021 Defratyka et al. installed a cavity ring down system (G2201-i, Picarro, Inc., USA) on a car and identified several methane sources in

Paris which increased the CH_4 concentration up to 2.7 parts per million (ppmV, 10^{-6}) (Defratyka et al., 2021). Elevations of CH_4 levels up to 88.6 ppmV were measured in Washington in 2014 by Jackson et al. (2014). This work reported a total of 5893 pipeline leaks over a distance of 1500 road miles, from which 1122 leaks increased the ambient CH_4 concentration to more than 5 ppmV and 67 leaks even over 25 ppmV. The threshold for leakage identification was proposed by von Fischer et al. who defined a 10% increase over the normal background concentration as a leakage (von Fischer et al., 2017). For a typical background concentration of about 2 ppmV, this corresponds to 200 ppbV. As an alternative to elaborate measurements in cities, low-cost devices with suitable CH_4 resolution (< 200 ppbV) could be installed at multiple locations and combined to a sensor network, which allows continuous remote leakage detection or emission monitoring. Photoacoustic (PA) gas sensors could meet these requirements of low-cost devices while retaining low enough detection limits. In PA the signal originates from converting vibrational energy of molecules into kinetic energy. A modulated light source electromagnetically excites the analyte of interest, which subsequently can release its additional vibrational energy as kinetic (translational) energy into the sample gas by colliding with surrounding molecules. This process is called vibrational-translational (VT) relaxation. The VT energy transfer increases the kinetic energy of the sample gas, causing the temperature to rise above its equilibrium value. Due to the modulation of the light source, the heat input induced by VT relaxation is also periodic, resulting in periodic density fluctuations, which per definition corresponds to a sound wave. By designing the optical path as an acoustic resonator, e.g. a cylindrical resonator, the photoacoustic sound wave can be amplified and filtered. The sound pressure linearly depends on the analyte concentration and may be detected by an acoustic-electric transducer, e.g. a microphone, quartz tuning fork (QTF) or a cantilever. Generally, the photoacoustically generated sound pressure amplitude p_{PA} for cylindrical resonators, excited in their first longitudinal mode can be described as follows (Miklós et al., 2001; Rück et al., 2023):

$$p_{\mathrm{PA}} = (\gamma - 1)\,\frac{Q}{f_{\mathrm{res}}}\,\frac{1}{2\pi^2 r^2}\,\frac{\mathrm{N_A}}{V_{\mathrm{mol}}}\,N_{\mathrm{i}}\sigma_{\mathrm{i}}\,(\lambda)\,P_0\varepsilon_{\mathrm{relax}} \tag{1}$$

The heat capacity ratio γ contains the number of all degrees of freedom (rotational, vibrational, translational) of the sample gas actively participating in sound propagation. Acoustic cross-sensitivities of the PA signal can be described by the ratio of the quality factor Q and the frequency f_{res} of acoustic resonance amplification. While r represents the radius of the resonator tube, $\mathrm{N_A}$ is the Avogadro constant, V_{mol} the molar volume of the sample gas, and N_{i} is the dimensionless volume fraction of the analyte with an absorption cross-section σ_{i} at the emitted wavelength λ. The optical power of the light source inside the photoacoustic measurement cell is designated as P_0. The efficiency of non-radiative relaxation is considered by $\varepsilon_{\mathrm{relax}}$, which is a quantity between 0 and 1. This quantity depends on the efficiency of all involved energy transitions of the gas mixture (Hunter et al., 1974). Chapter 2 briefly discusses the effect of non-radiative relaxation on the photoacoustic signal. Regarding photoacoustic methane detection recent literature provides several publications reporting ppbV - level limit of detection using infrared laser sources (Elefante et al., 2019, 2020; Giglio et al., 2020; Gong et al., 2021; Li et al., 2022; Xiao et al., 2022). In this work we present the results of a five day CH_4 measurement campaign in ambient air at the meteorological observatory of the German Weather Service (DWD) at Hohenpeißenberg with a photoacoustic sensor using a G2301 cavity ring down spectrometer as a reference. The photoacoustic sensor used in this work provides a limit of detection of 6.8 ppbV and will be briefly introduced in chapter 3.1 (for a detailed description see Pangerl et al. (2022)). The mountain Hohenpeißenberg (47.48°

N, 11.01° E) is located southwest of Munich at around 985 meters above sea level. Due to the naturally occurring fluctuations in ambient humidity during the measurement series, the relaxational behavior was significantly affected. Without including the algorithm CoNRad (see chapter 2) for data evaluation, no reasonable conclusions about the CH_4 concentration would be possible by the PA sensor. The intention of this paper is to demonstrate that the developed PA sensor in combination with the applied signal corrections provides an appropriate choice for reliable and ppbV-level-precise GHG monitoring. During the measuring campaign, the PA sensor does not show any trends in sensitivity (see Table 1), however, it is evident that it is advisable to calibrate the PA sensor frequently in order to maintain the accuracy of the sensor. The G2301, on the other hand, does not show any significant fluctuations in its methane calibration values.

2 Non-radiative relaxation in photoacoustic spectroscopy

The effect of variations in the non-radiative relaxation process is omnipresent in photoacoustic spectroscopy, e.g. Lang et al. (2020); Wysocki et al. (2006); Kalkman and van Kesteren (2008); Hayden et al. (2020); Qiao et al. (2022). Especially CH_4 is well-known to be prone to relaxational effects (Schilt et al., 2006; Barreiro et al., 2011, 2012; Elefante et al., 2020; Li et al., 2020; Menduni et al., 2020; Dello Russo et al., 2021; Müller et al., 2022; Pangerl et al., 2022; Rück et al., 2023). To compensate for signal losses due to incomplete relaxation we introduced an algorithm (CoNRad), which is discussed in detail in Müller et al. (2022). CoNRad can be used to predict the non-radiative relaxational behavior of the analyte, considering the composition, the pressure and the temperature of the sample gas. Starting from the laser excited energy state, CoNRad considers all relevant transitions originating from this state and calculates the individual efficiencies, as well as the released photoacoustic energy. The possibility to excite other energy states by collisions (vibrational - vibrational (VV) transition) is also considered by CoNRad. For a state excited by VV transition the same procedure is performed as for the initially excited state. This means that also from the VV excited state all relevant energy transitions as well as the released photoacoustic energy is computed. Once the ground state is reached, the individual energies are summed up resulting in the total photoacoustic energy. Consequently, CoNRad calculates the non-radiative relaxation efficiency $\varepsilon_{\text{relax}}$, which allows to predict the influence of different relaxation characteristics on the photoacoustic signal. In appendix Figure A1 the applied non-radiative relaxation cascade for methane in humid air is shown. The rates k of the individual collision reactions can be taken from Müller et al. (2022).

For an accurate description of the overall relaxation cascade in case of mid-infrared (MIR) - 2968.4 cm^{-1} methane monitoring in ambient air, i.e. mainly containing N_2, O_2 and H_2O, a total of 29 individual collision reactions have to be considered, according to Müller et al. (2022). In Figure 1(a) the overall relaxation efficiency $\varepsilon_{\text{relax}}$ at an acoustic frequency of 5055 Hz for methane diluted in air is plotted against continuous humidification of the sample. The data shown in Figure 1 was obtained via CoNRad (Müller et al., 2022). In dry air $\varepsilon_{\text{relax}}$ is only approximately 5.8 %, which implies that 94.2 % of the theoretically possible PA signal is lost due to delayed relaxation. The relaxation loss in case of methane in dry air is attributed to the strong coupling of the bending modes of methane ($2\nu_{\text{b,CH}_4}$ = 2844 cm^{-1} and $\nu_{\text{b,CH}_4}$ = 1422 cm^{-1}) with the vibrational state of oxygen ν_{O_2} = 1556 cm^{-1} (Schilt et al., 2006; Barreiro et al., 2011). This results in a fast vibrational-vibrational (VV) energy transfer

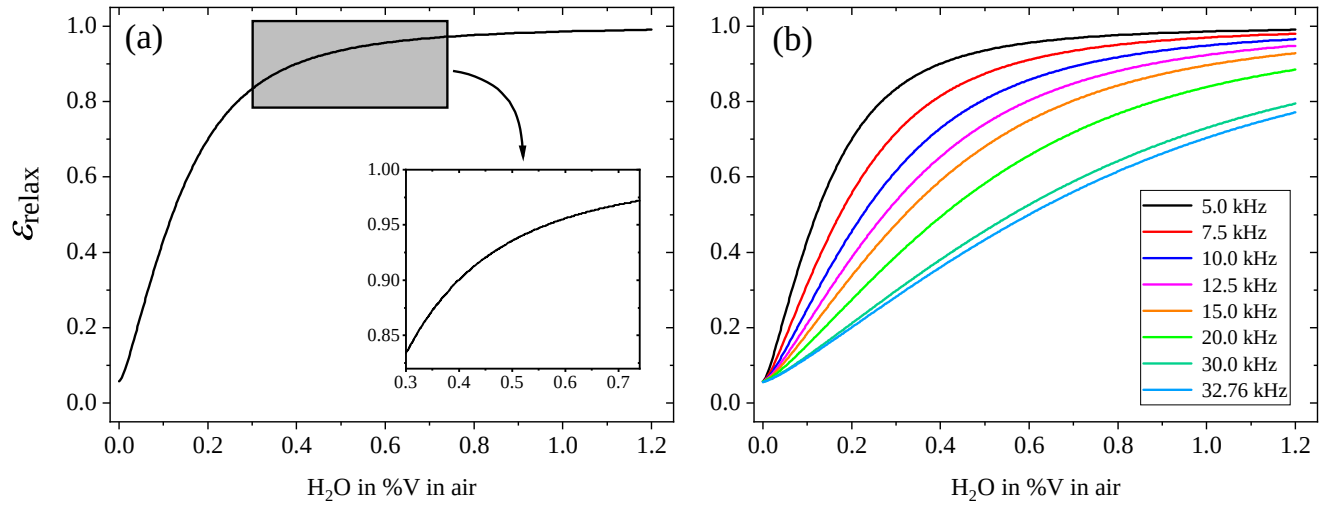

Figure 1. Overall efficiency of non-radiative relaxation ε_{relax} at 5055 Hz laser modulation for CH_4 in air with rising humidity content (a). The grey highlighted area in (a) indicates the observed humidity during the measurement period. The right side (b) displays how humidification of the sample affects ε_{relax} at different acoustic frequencies up to 32.76 kHz, which is a typical modulation frequency utilized in quartz-enhanced PA sensors (QEPAS).

from CH_4 to O_2. Oxygen, however, relaxes rather slow, causing the energy to accumulate in ν_{O_2}, and not contribute to PA signal generation, yielding a decrease of ε_{relax} (Schilt et al., 2006; Barreiro et al., 2011; Müller et al., 2022; Pangerl et al., 2022). The addition of humidity significantly increases the relaxation efficiency due to a fast VV energy transfer from ν_{O_2} to ν_{H_2O} = 1595 cm^{-1}, followed by a fast VT relaxation (Barreiro et al., 2012; Müller et al., 2022; Pangerl et al., 2022). The frequency dependency of the relaxation efficiency for methane is shown in Figure 1(b). The graphs demonstrate that with rising acoustic frequencies the relaxation losses become much more pronounced, yielding lower PA signals and thus worse detection limits.

3 Experimental

3.1 Photoacoustic sensor

An interband cascade laser (ICL) emitting at 2968.4 cm^{-1} with an optical power of 7.5 mW, after passing the photoacoustic measurement cell, excites the ν_{s1} stretching mode of CH_4 (absorption cross-section σ_{CH_4} = 4.9·10^{-19} cm^2mol^{-1}). Temperature, pressure and humidity within the PA cell were monitored by a BME280 (Bosch, Germany) TpH sensor. The PA cell is temperature controlled to 40 °C and operated in WM(2f) mode, i.e. the modulation frequency equals half the resonance frequency of the PA system. To prevent signal losses due to a mismatch of f_{res} and f_{mod}, the resonance properties of the PA sensor must be determined. Changes in the sample gas composition induce a change in f_{res}, as the speed of sound changes.

With the acoustic resonance monitoring system (ARMS) as presented in Rück et al. (2023) an integrated, fast and accurate quantification of the acoustic properties of PA cells was introduced and utilized in this work. This technique additionally allows for Q - factor quantification, which directly affects the generated PA pressure p_{PA}, see equation 1. Together the with the simulated non-radiative relaxation efficiency $\varepsilon_{\mathrm{relax}}$, P_0, the measured Q - factor and resonance frequency f_{res} and the calculated heat capacity ratio γ the raw photoacoustic signal $U_{\mathrm{PA,\,raw}}$ in μV is compensated after equation (2), yielding the final methane concentration output of the PA sensor $\mathrm{CH}_{4,\mathrm{PA}}$.

$$\mathrm{CH}_{4,\mathrm{PA}} = \frac{U_{\mathrm{PA,\,raw}}}{S_{\mathrm{cali}}} \cdot \frac{\varepsilon_{\mathrm{relax,\,cali}}}{\varepsilon_{\mathrm{relax}}} \cdot \frac{Q_{\mathrm{cali}}}{Q} \cdot \frac{f_{\mathrm{res}}}{f_{\mathrm{res,\,cali}}} \cdot \frac{(\gamma_{\mathrm{cali}} - 1)}{(\gamma - 1)} \cdot \frac{P_{0,\mathrm{cali}}}{P_0} \tag{2}$$

The quantities labeled with *cali* in the index were obtained during the respective calibration measurements, with the calibration sensitivity S_{cali} in $\mu\mathrm{V/ppmV}$. For comparison purpose the sensitivity S in Table 1 is normalized to a humidity of $0.3\,\%\mathrm{V}$.

3.2 Measurement setup

The measurement setup is visualized in Figure 2. Ambient air was sampled by means of a pump from outside the laboratory. A three-way valve was used to automatically switch between reference gas and ambient air. Dry natural air was chosen as the reference gas, which consists mostly of N_2 and O_2 but also includes noble gases as well as trace gases (CH_4, CO_2, N_2O, CO). The reference gas tank was filled and calibrated by the ICOS Flask and Calibration Laboratory (FCL) and is linked to the WMO X2004A scale, which provides 2020 ppbV CH_4 with an uncertainty below 0.5 ppbV (Jordan and Schumacher, 2022). During the measurement campaign, the reference gas was used a total of seven times for 30 minutes per interval to avoid and detect potential sensor drifts, see Table 1. As the difference between the theoretical calculations of CoNRad and the measured data is highest for only slightly humidified measuring environments ($H_2O < 0.25\,\%\mathrm{V}$), see Figure 11 from Müller et al. (2022), an additional humidification of the sample gases of about $0.3\,\%\mathrm{V}$ was chosen to avoid this issue. This was realized by a humidity generator installed up-stream of the PA sensor. A lock-in-amplifier (LIA) time constant of τ_{LIA} = 20 s was chosen to reduce the effect of white noise on the PA data. Every 10 minutes the PA sensor recorded three single point measurements (SPMs) each for 20 s with a data acquisition rate of 5 Hz. The three SPMs themselves where further averaged, as well as the individual standard deviations, yielding the final values. The ARMS routine was performed to determine Q and f_{res} each time before the three SPMs were recorded. Based on the ARMS, the modulation frequency of the laser was automatically adjusted, while the PA ICL was switched off between the measurements. According to equation (2) the raw photoacoustic signal was corrected for variations in $\varepsilon_{\mathrm{relax}}$, γ, Q, f_{res} and P_0. As shown in Figure 2 the G2301, operated with a data acquisition rate of 0.2 Hz and an averaging time of 5 s, was installed in the gas setup parallel to the PA sensor, ensuring that both devices received the same sample gas, providing comparability of the sensor readings.

4 Results and discussion

The data of the PA sensor during reference gas measurements are summarized in Table 1. The sensitivity of the PA sensor varies only slightly (maximum -2.61 % from the average value), which demonstrates the stability of the photoacoustic system, but still

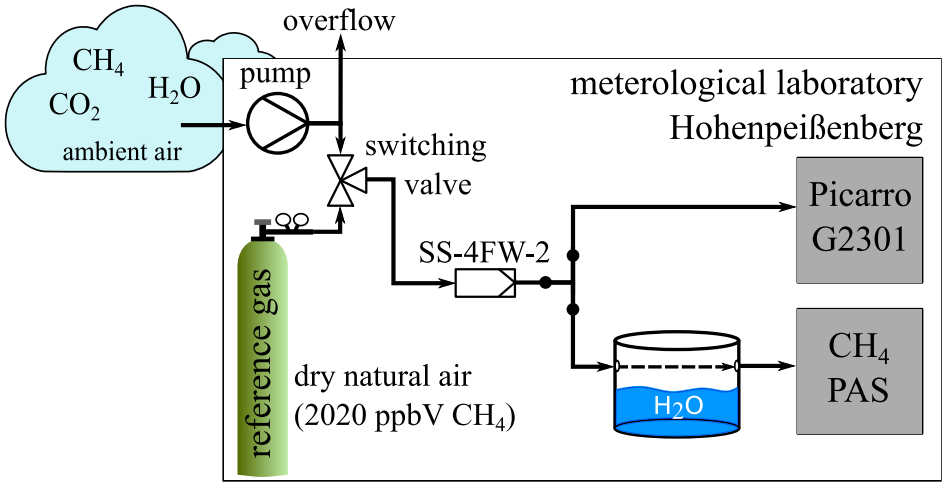

Figure 2. Schematic of the experimental setup for the measurement campaign. The pump delivers ambient air from outside the laboratory. A three-way valve is used to switch between ambient air and reference gas. The reference gas consists of 2020 ppbV methane in dry natural air. Before the respective sample gas is fed into the two measurement instruments, it passes a stainless steel filter (SS-4FW-2) to avoid particle contamination.

show the necessity for frequent calibration to ensure high accuracy. While the mean CH_4 precision $3\sigma_{PAS}$ = 6.75 ppbV is worse than the observed precision of the reference ($3\sigma_{G2301}$ = 1.16 ppbV), the PA sensor is nevertheless sufficiently precise to reliably detect the atmospheric CH_4 fluctuations, refer to Figure 3(a). Figure 3 illustrates the CH_4 readings in ppbV (a) obtained by the PA sensor, including the previously mentioned signal corrections (black) and the G2301 data (red), respectively. The grey dashed lines indicate a new day. It is obvious, that the CH_4 concentration characteristics monitored with both devices agree quite well with each other. However, more significant discrepancies up to > $\pm$80 ppbV, are also evident. As of now no clear explanation could be identified for these deviations. It is unlikely that these errors are induced by differences in the sample gas of the two systems since the humidity readings of the BME280 integrated in the PA sensor match very well with the readings of the G2301, as shown in Figure 3(c). By evaluating the data acquisition system (DAS), cavity, and etalon temperature of the Picarro G2301 temporal anomalies regarding CH_4 discrepancies could be identified (see Figure B1).

Since the temperature spikes are probably caused by direct sunlight on the G2301, it is recommended to avoid this for similar experiments. Still, the average percentage deviation of the PA sensor and the G2301 reference of 1.11 % is rather moderate, see Figure 3(b).

Over the entire period of the measurement campaign, the water content in the PA sample gas varied from about 0.30 %V to about 0.73 %V, see Figure 3(c), causing the raw PA sensor readings to alter by about 13.5 % due to relaxational effects, refer to Figure 1(a), which makes standard calibration unfeasible. For this reason, algorithmic compensation methods like CoNRad are essential. The Q-factor, f_{res} and P_0 remained virtually constant during the measurement period. Also the variation of γ induced by fluctuating humidity was negligible compared to the relaxational effect. Figure 4 illustrates the impact of CoNRad

calibration	PAS sensitivity S in μV/ppmV	3σ precision in nV	3σ precision in ppbV	G2301 in ppbV	3σ G2301 in ppbV
#1	2.08	14.14	6.80	2019.99	0.96
#2	2.12	22.50	10.61	2020.13	0.72
#3	2.13	7.18	3.37	2019.70	0.92
#4	2.16	8.59	3.98	2019.88	0.86
#5	2.14	17.91	8.37	2020.07	2.04
#6	2.16	14.93	6.91	2019.67	1.52
#7	2.15	15.56	7.24	2019.61	1.04

Table 1. Sensitivity S of the PA sensor, normalized to a sample humidity of 0.3 %V, over the five day measurement period. An average deviation of 0.98 % and a maximum deviation of -2.61 % from the mean of the observed sensitivities show the stability of the PA sensor. The long-term accuracy as well as the precision of the G2301 are listed in the two right columns. The campaign started on 6 February 2023 afternoon and ended on 10 February 2023 morning.

on the reliability of PA sensor readings. The y-axis represents the difference between the CH_4 concentration readings of the PA sensor and that of the G2301 in ppbV. The grey dashed lines again indicate a new day. The black curve in Figure 4(a) shows the deviation when CoNRad is implemented $(\Delta\mathrm{CH_4}\,(\mathrm{PA_{CoNRad}} - \mathrm{G2301}))$ in the data evaluation, the red curve illustrates the deviation based on the raw PA data $(\Delta\mathrm{CH_4}\,(\mathrm{PA_{raw}} - \mathrm{G2301}))$. This red curve illustrates, that due to the exponential effect of relaxation processes, the offset between raw data and the reference measurement is not constant. The grey highlighted data in Figure 4 show the results for dry PA reference gas operation, with the empty humidity tank during 9$^{\mathrm{th}}$ of February. Without CoNRad dry calibration leads to considerable misinterpretations of the PA data. Thus ambient CH_4 PAS monitoring without algorithmic compensation approaches is not possible. Figure 4(b) shows a statistical evaluation of the absolute differences. It indicates that with CoNRad the variance of the measured deviation with respect to the reference decreases significantly. In addition, the compensated values show normal distribution around 5.26 ppbV, indicating no long-term drift. The raw values, however, are not normally distributed and show a substantially higher variance. The large deviation of about 1000 ppmV CH_4 of the raw PA data (grey highlighted area) can be attributed to dry reference gas mode, in which pronounced relaxational losses occur, see Figure 1.

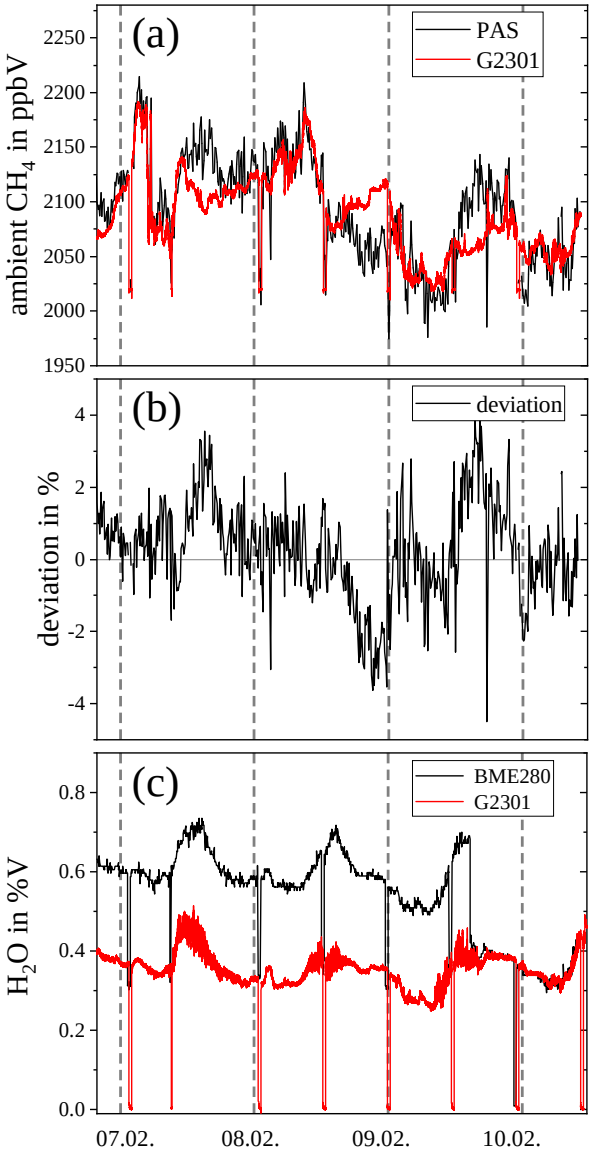

Figure 3. Direct comparison of the methane concentration readings (a), the deviation of the PA sensor compared to the Picarro G2301 in % (b) and the water readings (c). The humidity offset induced by the measurement setup is clearly visible. During 09.02. the humidity tank became empty, resulting in no additional humidification.

5 Conclusions

We compared our PA methane gas sensor with an established and calibrated cavity ringdown spectrometer (G2301) used for global GHG monitoring. Over a period of five days, ambient air has been monitored at the meteorological observatory

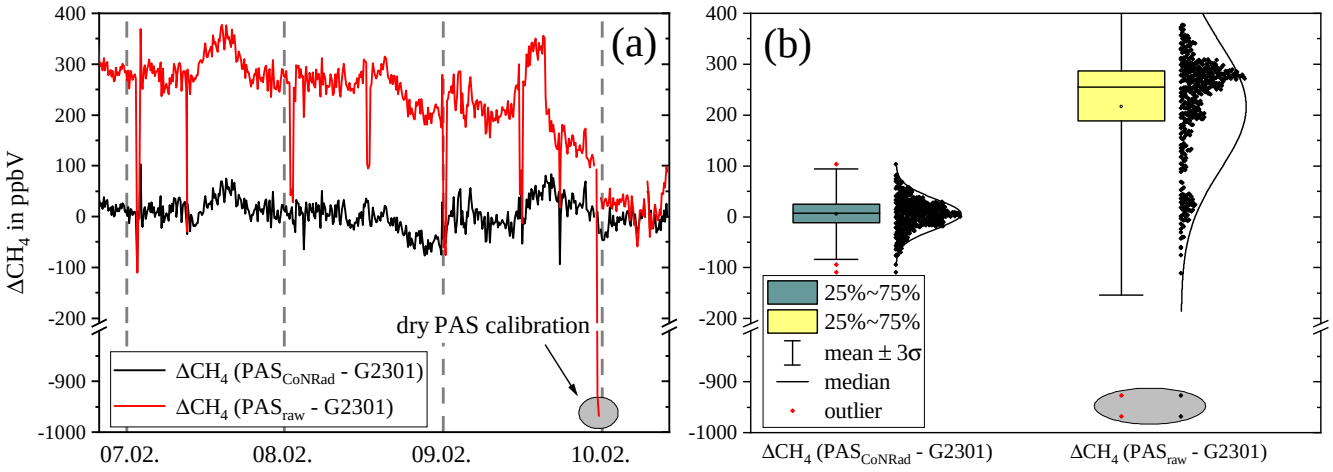

Figure 4. Absolute difference of CH_4 in ppbV (a) based on raw PA data (red) and after CoNRad compensation (black) with regard to the G2301 reference methane readings. The right side (b) displays the boxplots and histograms of the deviations. The grey highlighted data indicates dry PAS calibration without CoNRad compensation.

Hohenpeißenberg of the DWD by both systems. The obtained results demonstrate that the PA sensor (3σ precision = 6.75 ppbV) is able to detect even small natural methane fluctuations in ambient air, thus providing an alternative to established devices. Further applications of the sensor would cover natural gas leakage detection, identification of new methane sources, or emission monitoring from agriculture or landfills. Generally photoacoustic systems provide low detection limits and high potential for miniaturization, however, relaxation-induced signal alterations pose a major drawback of this technique. The counteracting water and oxygen induced relaxation effects play an important role in ambient photoacoustic methane detection, as highlighted in this work. Only in environments with clearly defined and constant measurement matrix, e.g. contamination measurement of high purity gases, the effect of relaxation on the photoacoustic signal may be neglected. For measurement applications with varying gas composition, e.g. fluctuating ambient humidity, PA devices essentially require the implementation of algorithmic models, such as CoNRad, in order to compensate for signal losses due to delayed relaxation that otherwise might cause significant errors in PA sensor data. The combination of CoNRad to simulate the non-radiative relaxational cascade and ARMS for real-time monitoring of Q and f_{res}, allows for reliable analyte concentration readings with photoacoustic sensors.

Code availability. The source code is available upon reasonable request. Please contact Max Müller (max.mueller@oth-regensburg.de) or Thomas Rück (thomas.rueck@oth-regensburg.de)

Data availability. For data related to this paper please contact Max Müller (max.mueller@oth-regensburg.de)

Appendix A: appendix

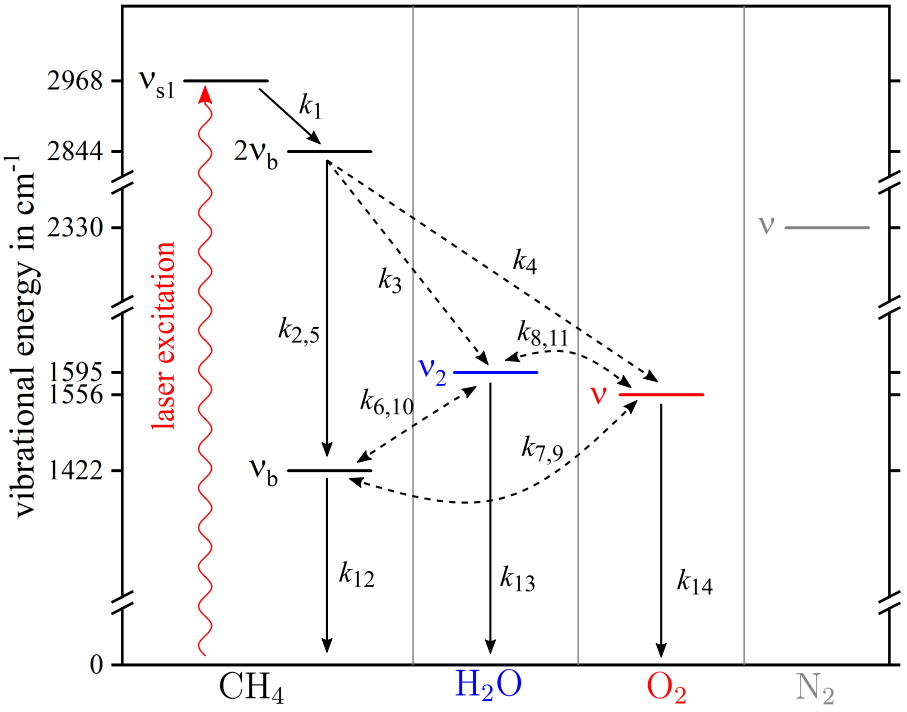

Figure A1. Jablonsky diagram of the non-radiative relaxation of methane in humid air, after (Müller et al., 2022). The rate constants k of the individual transitions can be found in (Müller et al., 2022). The influence of traces of CO_2 on the relaxational behaviour can be neglected (Rück et al., 2023).

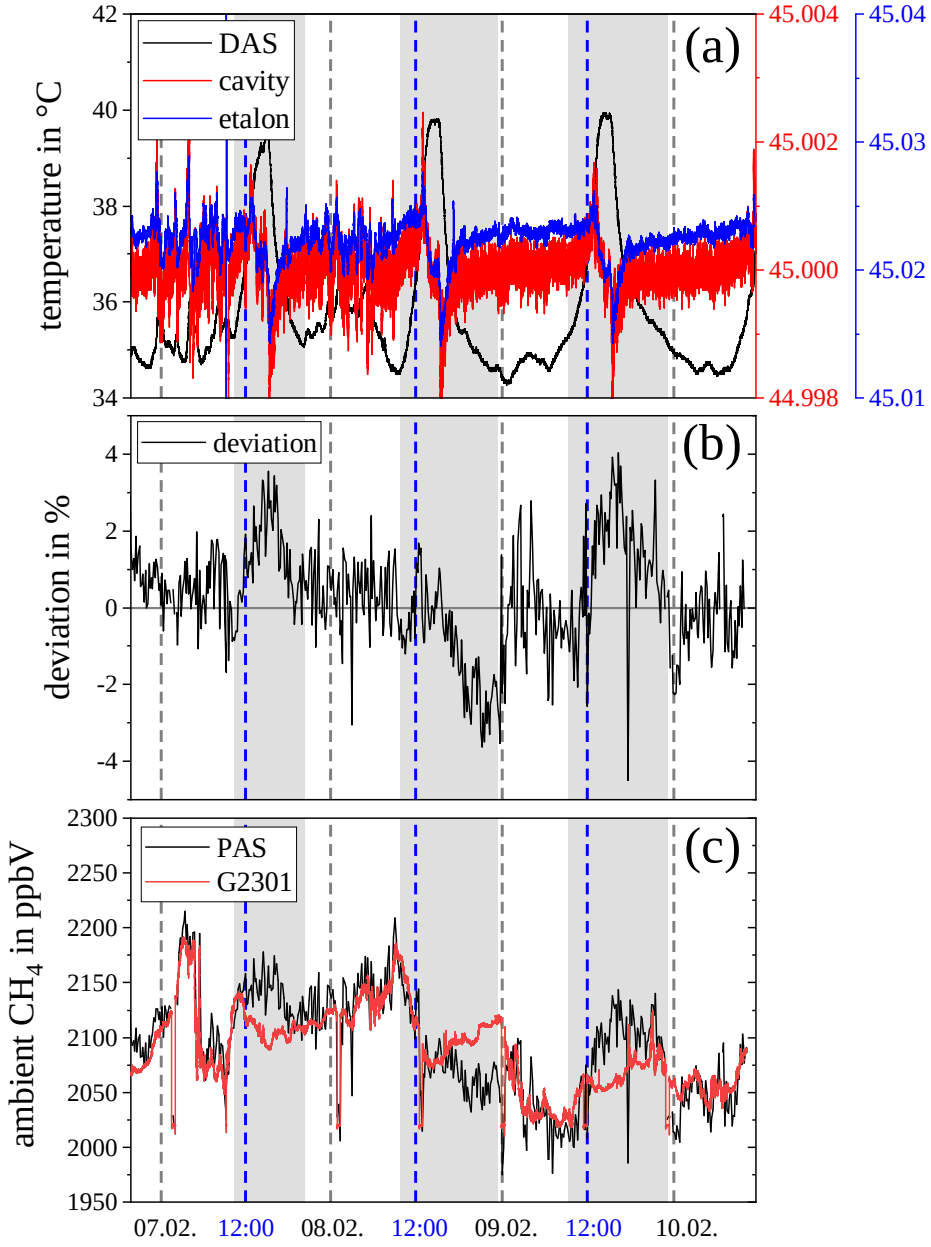

Figure B1. Comparison of data acquisition system (DAS), cavity and etalon temperature (a) of the Picarro G2301 CRDS over time, with the measured percentage deviation (b) and CH_4 reading (c). The temperature spikes (grey highlighted areas) seem to correlate with the strongest deviations. The blue dashed lines indicate noon, which leads to the assumption that such spikes in temperature may be caused by direct sun exposure of the device.

Author contributions. **Max Müller**: Conceptualization, Data curation, Investigation, Methodology, Software,Writing – original draft, Writing – review & editing. **Stefan Weigl**: Conceptualization, Data curation, Investigation, Methodology, Software,Writing – review & editing. **Jennifer Müller-Williams**: Conceptualization, Data curation, Investigation, Methodology, Writing – review & editing. **Matthias Lindauer**: Conceptualization, Data curation, Investigation, Methodology, Writing – review & editing. **Thomas Rück**: Methodology, Software, Validation, Funding acquisition, Writing – review & editing. **Simon Jobst**: Methodology, Software, Validation, Writing – review & editing. **Rudolf Bierl**: Funding acquisition, Project administration, Supervision, Validation, Writing – review & editing. **Frank-Michael Matysik**: Conceptualization, Methodology, Supervision, Validation, Writing – review & editing.

Competing interests. The authors declare that they have no conflict of interest.

Acknowledgements. This work was financially supported by the project PreSEDA funded by the German government and the Federal Ministry of Economic Affairs and Energy (BMWi). The funding code of PreSEDA is 03EN2028A.

References

Barreiro, N., Vellespi, A., Santiago, G., Slezak, V., and Peuriot, A.: Influence of oxygen on the resonant photoacoustic signal from methane excited at the $\nu 3$ mode, Applied Physics B, 104, 983–987, https://doi.org/https://doi.org/10.1007/s00340-011-4546-8, 2011.

Barreiro, N., Peuriot, A., Santiago, G., and Slezak, V.: Water-based enhancement of the resonant photoacoustic signal from methane–air samples excited at 3.3 μm, Applied Physics B, 108, 369–375, https://doi.org/https://doi.org/10.1007/s00340-012-5018-5, 2012.

Defratyka, S. M., Paris, J.-D., Yver-Kwok, C., Fernandez, J. M., Korben, P., and Bousquet, P.: Mapping Urban Methane Sources in Paris, France, Environmental Science & Technology, 55, 8583–8591, https://doi.org/10.1021/acs.est.1c00859, pMID: 34159780, 2021.

Dello Russo, S., Sampaolo, A., Patimisco, P., Menduni, G., Giglio, M., Hoelzl, C., Passaro, V. M., Wu, H., Dong, L., and Spagnolo, V.: Quartz-enhanced photoacoustic spectroscopy exploiting low-frequency tuning forks as a tool to measure the vibrational relaxation rate in gas species, Photoacoustics, 21, 100 227, https://doi.org/https://doi.org/10.1016/j.pacs.2020.100227, 2021.

Elefante, A., Giglio, M., Sampaolo, A., Menduni, G., Patimisco, P., Passaro, V. M., Wu, H., Rossmadl, H., Mackowiak, V., Cable, A., Tittel, F. K., Dong, L., and Spagnolo, V.: Dual-Gas Quartz-Enhanced Photoacoustic Sensor for Simultaneous Detection of Methane/Nitrous Oxide and Water Vapor, Analytical Chemistry, 91, 12 866–12 873, https://doi.org/10.1021/acs.analchem.9b02709, pMID: 31500409, 2019.

Elefante, A., Menduni, G., Rossmadl, H., Mackowiak, V., Giglio, M., Sampaolo, A., Patimisco, P., Passaro, V. M. N., and Spagnolo, V.: Environmental Monitoring of Methane with Quartz-Enhanced Photoacoustic Spectroscopy Exploiting an Electronic Hygrometer to Compensate the H2O Influence on the Sensor Signal, Sensors, 20, https://doi.org/10.3390/s20102935, 2020.

Giglio, M., Zifarelli, A., Sampaolo, A., Menduni, G., Elefante, A., Blanchard, R., Pfluegl, C., Witinski, M. F., Vakhshoori, D., Wu, H., Passaro, V. M., Patimisco, P., Tittel, F. K., Dong, L., and Spagnolo, V.: Broadband detection of methane and nitrous oxide using a distributed-feedback quantum cascade laser array and quartz-enhanced photoacoustic sensing, Photoacoustics, 17, 100 159, https://doi.org/https://doi.org/10.1016/j.pacs.2019.100159, 2020.

Gong, Z., Gao, T., Mei, L., Chen, K., Chen, Y., Zhang, B., Peng, W., and Yu, Q.: Ppb-level detection of methane based on an optimized T-type photoacoustic cell and a NIR diode laser, Photoacoustics, 21, 100 216, https://doi.org/https://doi.org/10.1016/j.pacs.2020.100216, 2021.

Hayden, J., Baumgartner, B., and Lendl, B.: Anomalous Humidity Dependence in Photoacoustic Spectroscopy of CO Explained by Kinetic Cooling, Applied Sciences, 10, https://doi.org/10.3390/app10030843, 2020.

Hunter, T. F., Rumbles, D., and Stock, M. G.: Photophysical processes in the vapour-phase measured by the optic-acoustic effect. Part 1.—The model and apparatus for the study of radiationless processes, J. Chem. Soc., Faraday Trans. 2, 70, 1010–1021, https://doi.org/10.1039/F29747001010, 1974.

ICOS RI: ICOS Atmosphere Station Specifications V2.0 (editor: O. Laurent), https://doi.org/10.18160/GK28-2188, 2020.

Jackson, R. B., Down, A., Phillips, N. G., Ackley, R. C., Cook, C. W., Plata, D. L., and Zhao, K.: Natural Gas Pipeline Leaks Across Washington, DC, Environmental Science & Technology, 48, 2051–2058, https://doi.org/10.1021/es404474x, pMID: 24432903, 2014.

Jordan, A. and Schumacher, M.: ICOS CAL - Quality Control Report 2021, https://doi.org/10.18160/RS2Q-RA1Q, 2022.

Kalkman, J. and van Kesteren, H.: Relaxation effects and high sensitivity photoacoustic detection of NO2 with a blue laser diode, Applied Physics B, 90, 197–200, https://doi.org/https://doi.org/10.1007/s00340-007-2895-0, 2008.

Lang, B., Breitegger, P., Brunnhofer, G., Valero, J., Schweighart, S., Klug, A., Hassler, W., and Bergmann, A.: Molecular relaxation effects on vibrational water vapor photoacoustic spectroscopy in air, Applied Physics B, 126, https://doi.org/https://doi.org/10.1007/s00340-020-7409-3, 2020.

Li, Y., Wang, R., Tittel, F. K., and Ma, Y.: Sensitive methane detection based on quartz-enhanced photoacoustic spectroscopy with a high-power diode laser and wavelet filtering, Optics and Lasers in Engineering, 132, 106 155, https://doi.org/https://doi.org/10.1016/j.optlaseng.2020.106155, 2020.

Li, Z., Liu, J., Si, G., Ning, Z., and Fang, Y.: Design of a high-sensitivity differential Helmholtz photoacoustic cell and its application in methane detection, Opt. Express, 30, 28 984–28 996, https://doi.org/10.1364/OE.465161, 2022.

Menduni, G., Sgobba, F., Russo, S. D., Ranieri, A. C., Sampaolo, A., Patimisco, P., Giglio, M., Passaro, V. M., Csutak, S., Assante, D., Ranieri, E., Geoffrion, E., and Spagnolo, V.: Fiber-Coupled Quartz-Enhanced Photoacoustic Spectroscopy System for Methane and Ethane Monitoring in the Near-Infrared Spectral Range, Molecules, 25, https://doi.org/10.3390/molecules25235607, 2020.

Miklós, A., Hess, P., and Bozóki, Z.: Application of acoustic resonators in photoacoustic trace gas analysis and metrology, Review of Scientific Instruments, 72, 1937–1955, https://doi.org/10.1063/1.1353198, 2001.

Müller, M., Rück, T., Jobst, S., Pangerl, J., Weigl, S., Bierl, R., and Matysik, F.-M.: An Algorithmic Approach to Compute the Effect of Non-Radiative Relaxation Processes in Photoacoustic Spectroscopy, Photoacoustics, 26, 100 371, https://doi.org/https://doi.org/10.1016/j.pacs.2022.100371, 2022.

Pangerl, J., Müller, M., Rück, T., Weigl, S., and Bierl, R.: Characterizing a sensitive compact mid-infrared photoacoustic sensor for methane, ethane and acetylene detection considering changing ambient parameters and bulk composition (N2, O2 and H2O), Sensors and Actuators B: Chemical, 352, 130 962, https://doi.org/https://doi.org/10.1016/j.snb.2021.130962, 2022.

Qiao, Y., Tang, L., Gao, Y., Han, F., Liu, C., Li, L., and Shan, C.: Sensitivity enhanced NIR photoacoustic CO detection with SF6 promoting vibrational to translational relaxation process, Photoacoustics, 25, 100 334, https://doi.org/https://doi.org/10.1016/j.pacs.2022.100334, 2022.

Rück, T., Müller, M., Jobst, S., Weigl, S., Pangerl, J., Bierl, R., and Matysik, F.-M.: Digital Twin of a photoacoustic trace gas sensor for monitoring methane in complex gas compositions, Sensors and Actuators B: Chemical, 378, 133 119, https://doi.org/https://doi.org/10.1016/j.snb.2022.133119, 2023.

Schilt, S., Besson, J.-P., and Thevenaz, L.: Near-infrared laser photoacoustic detection of methane: the impact of molecular relaxation, Applied Physics B, 82, 319–328, https://doi.org/https://doi.org/10.1007/s00340-005-2076-y, 2006.

von Fischer, J. C., Cooley, D., Chamberlain, S., Gaylord, A., Griebenow, C. J., Hamburg, S. P., Salo, J., Schumacher, R., Theobald, D., and Ham, J.: Rapid, Vehicle-Based Identification of Location and Magnitude of Urban Natural Gas Pipeline Leaks, Environmental Science & Technology, 51, 4091–4099, https://doi.org/10.1021/acs.est.6b06095, pMID: 28326761, 2017.

Wysocki, G., Kosterev, A., and Tittel, F.: Influence of molecular relaxation dynamics on quartz-enhanced photoacoustic detection of CO2 at λ =2 μm, Applied Physics B, 85, 301–306, https://doi.org/https://doi.org/10.1007/s00340-006-2369-9, 2006.

Xiao, H., Zhao, J., Sima, C., Lu, P., Long, Y., Ai, Y., Zhang, W., Pan, Y., Zhang, J., and Liu, D.: Ultra-sensitive ppb-level methane detection based on NIR all-optical photoacoustic spectroscopy by using differential fiber-optic microphones with gold-chromium composite nanomembrane, Photoacoustics, 26, 100 353, https://doi.org/https://doi.org/10.1016/j.pacs.2022.100353, 2022.